Fluorine-19 NMR and computational quantification of isoflurane binding to the voltage-gated sodium channel NaChBac

Monica N. Kinde[a,1], Vasyl Bondarenko[a,1], Daniele Granata[b], Weiming Bu[c], Kimberly C. Grasty[d], Patrick J. Loll[d], Vincenzo Carnevale[b], Michael L. Klein[b,2], Roderic G. Eckenhoff[c], Pei Tang[a,e,f], and Yan Xu[a,e,g,2]

[a]Department of Anesthesiology, University of Pittsburgh School of Medicine, Pittsburgh, PA 15261; [b]Institute for Computational Molecular Science, College of Science and Technology, Temple University, Philadelphia, PA 19122; [c]Department of Anesthesiology & Critical Care, University of Pennsylvania Perelman School of Medicine, Philadelphia, PA 19104; [d]Department of Biochemistry and Molecular Biology, Drexel University College of Medicine, Philadelphia, PA 19102; [e]Department of Pharmacology and Chemical Biology, University of Pittsburgh School of Medicine, Pittsburgh, PA 15261; [f]Department of Computational and Systems Biology, University of Pittsburgh School of Medicine, Pittsburgh, PA 15261; and [g]Department of Structural Biology, University of Pittsburgh School of Medicine, Pittsburgh, PA 15261

Contributed by Michael L. Klein, October 11, 2016 (sent for review June 23, 2016; reviewed by Edward J. Bertaccini and Emad Tajkhorshid)

Voltage-gated sodium channels (Na_V) play an important role in general anesthesia. Electrophysiology measurements suggest that volatile anesthetics such as isoflurane inhibit Na_V by stabilizing the inactivated state or altering the inactivation kinetics. Recent computational studies suggested the existence of multiple isoflurane binding sites in Na_V, but experimental binding data are lacking. Here we use site-directed placement of ^{19}F probes in NMR experiments to quantify isoflurane binding to the bacterial voltage-gated sodium channel NaChBac. ^{19}F probes were introduced individually to S129 and L150 near the S4–S5 linker, L179 and S208 at the extracellular surface, T189 in the ion selectivity filter, and all phenylalanine residues. Quantitative analyses of ^{19}F NMR saturation transfer difference (STD) spectroscopy showed a strong interaction of isoflurane with S129, T189, and S208; relatively weakly with L150; and almost undetectable with L179 and phenylalanine residues. An orientation preference was observed for isoflurane bound to T189 and S208, but not to S129 and L150. We conclude that isoflurane inhibits NaChBac by two distinct mechanisms: (*i*) as a channel blocker at the base of the selectivity filter, and (*ii*) as a modulator to restrict the pivot motion at the S4–S5 linker and at a critical hinge that controls the gating and inactivation motion of S6.

general anesthetics | drug–protein interaction | voltage-gated sodium channel | nuclear magnetic resonance | molecular dynamics simulation

General anesthetics disrupt sensory communications by modulating proteins in the central nervous system (1–4). For many years, the physiological relevance of a protein class to general anesthesia has been judged based on the protein's sensitivity to anesthetics, particularly the steepness of the in vitro concentration dependence, in comparison with that of the in vivo dose–responses. This phenomenological reasoning has led to the belief that voltage-gated Na^+ and K^+ channels, with the exception of the two-pore K^+ channel, are unlikely to play a substantial role in general anesthesia due to their gradual dose–response to volatile anesthetics (5). A new theory on the percolation of sensory information in the brain suggests that the steepness of the in vivo anesthesia dose–response curve is the result of a phase transition in the stochastic information access on a global scale, independent of deterministic connections among different neurons or brain regions (1). Thus, any interference with sensory communications, even with a gradual dose–response, can contribute to the overall dynamics of the steep phase transition. In this regard, voltage-gated Na^+ channels (Na_V) are likely to be a relevant molecular target for general anesthetics (6, 7). Consistent with enhanced inhibition of fast firing neurons, volatile anesthetics may inhibit neurotransmitter release through action on presynaptic Na_V, stabilize the fast-inactivated state of neuronal Na_V, and depress Na^+ current during high-frequency stimulation (8, 9). All of these actions contribute to the disruptions of normal sensory processes by decreasing the probability for information integration through axonal and synaptic communications.

The bacterial voltage-gated sodium channel NaChBac is a homolog of eukaryotic Na_V. It shares with Na_V a similar pharmacological profile in response to volatile anesthetics, such as isoflurane, which inhibits inward currents of NaChBac in a concentration-dependent manner (10). The ease with which NaChBac can be produced in large quantity and high purity makes it a suitable model for high-resolution structural and functional studies of anesthetic binding in voltage-gated ion channels (11, 12).

In silico screening of isoflurane binding sites and access pathways in NaChBac was performed previously on a closed-pore NaChBac structure model through molecular dynamics "flooding" simulations (12). Three regions, including the central cavity in the pore, the S4–S5 linker, and the extracellular surface of the channel near the selectivity filter, were identified. The simulations suggest that isoflurane binding affinities at these sites are physiologically relevant (12). All three regions are predicted to be important for channel gating and conduction. Despite the thorough computational investigations, no experimental analyses have been performed to characterize isoflurane binding to NaChBac with high structural resolution.

Significance

How general anesthetics modulate the function of voltage-gated sodium (Na_V) channels remains a mystery. Here, strategic placements of ^{19}F probes, guided by molecular dynamics simulations, allowed for high-resolution NMR quantitation of the volatile anesthetic isoflurane binding to the bacterial Na_V channel NaChBac. The data provided experimental evidence showing that channel blockade at the base of the ion selectivity filter and the restricted pivot motion at the S4–S5 linker and the P2–S6 helix hinge underlie the action of isoflurane on NaChBac. The results contribute to a better understanding of the molecular mechanisms of general anesthesia.

Author contributions: M.L.K., P.T., and Y.X. designed research; M.N.K., V.B., D.G., W.B., K.C.G., and V.C. performed research; P.J.L., V.C., M.L.K., R.G.E., P.T., and Y.X. contributed new reagents/analytic tools; M.N.K., V.B., D.G., V.C., M.L.K., P.T., and Y.X. analyzed data; and M.N.K., D.G., V.C., P.T., and Y.X. wrote the paper.

Reviewers: E.J.B., Stanford University and VA Palo Alto Health Care System; and E.T., University of Illinois at Urbana–Champaign.

The authors declare no conflict of interest.

Freely available online through the PNAS open access option.

[1]M.N.K. and V.B. contributed equally to this work.

[2]To whom correspondence may be addressed. Email: mlklein@temple.edu or xuy@anes.upmc.edu.

This article contains supporting information online at www.pnas.org/lookup/suppl/doi:10.1073/pnas.1609939113/-/DCSupplemental.

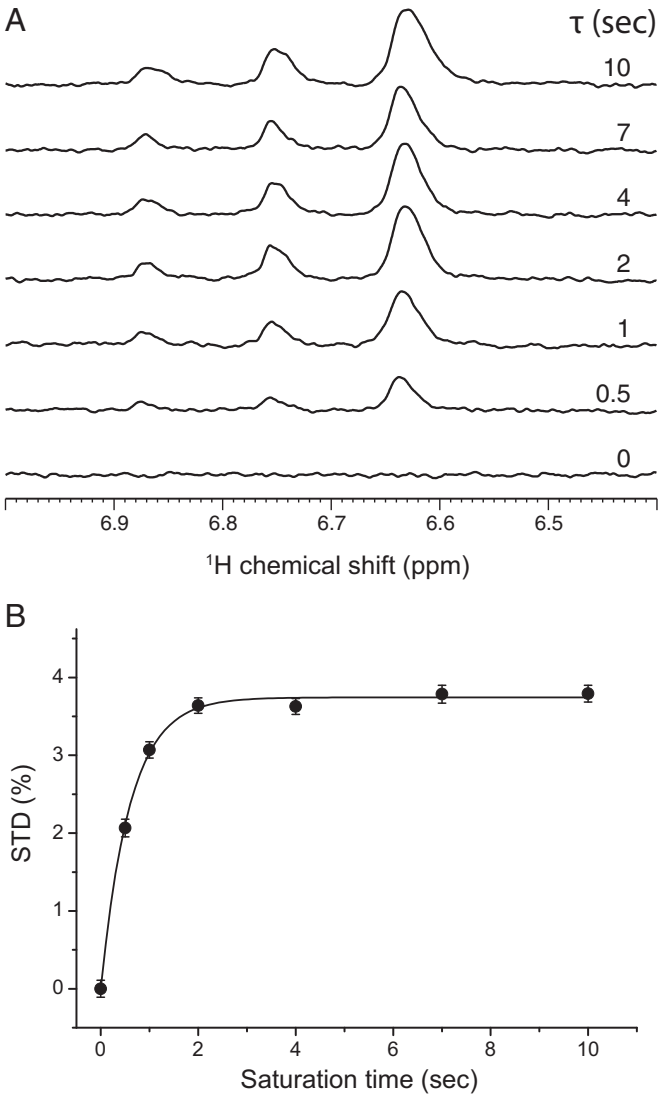

Fig. 1. ^{1}H STD NMR determination of isoflurane interaction with NaChBac. (*A*) The ^{1}H STD spectra for the region of isoflurane (CF_3-CHCl-O-CHF_2) resonances at different saturation times as indicated in the figure. The sample contained NaChBac (50 μM) and isoflurane (1.1 mM). Each STD spectrum was obtained by subtracting a pair of spectra acquired in an interleaved fashion with on- and off-resonance frequencies of 0.4 and 25 ppm, respectively ($V_{STD} = V_{off} - V_{on}$). The –CHCl– proton of isoflurane has a single peak centered at 6.63 ppm; the $-CHF_2$ proton has triplet peaks centered at 6.75 ppm with one of the peaks overlapping with the –CHCl– peak. ^{1}H chemical shifts were referenced to the 4,4-dimethyl-4-silapentane-1-sulfonic acid resonance at 0 ppm. (*B*) STD (%) of isoflurane as a function of the saturation time. STD (%) values were calculated based on $(V_{off} - V_{on})/V_{off} \times 100\%$, where V_{off} and V_{on} were signal integrals of isoflurane in the off- and on-resonance saturation transfer spectra, respectively. Experimental STD (%) values were fit to Eq. **1** as outlined in *Methods*. Uncertainties in STD (%) were determined by the NMR signal intensity and noise level. At a longer saturation time, STD (%) reached a steady-state regime.

Experimentally, saturation transfer difference (STD) NMR spectroscopy is a powerful approach to identifying and characterizing ligand binding in proteins (13, 14), and is particularly suitable for investigations of anesthetic–protein interactions due to the low-affinity nature of the anesthetic binding (15). In this study, we used NMR—particularly, homonuclear ^{19}F STD spectroscopy—to characterize site-specific isoflurane binding in NaChBac. Isoflurane was found to bind to several regions in NaChBac with different affinities. The results provide a structural basis for understanding isoflurane inhibitory effects on the function of NaChBac and other homologous sodium channels.

Results

Isoflurane Interacts Directly with NaChBac. Before any systematic mutagenesis studies, we first performed ^{1}H-NMR STD experiments to determine whether isoflurane interacts directly with NaChBac. The isoflurane ^{1}H STD signals increased with saturation times (Fig. 1*A*), an indication of direct interactions between isoflurane and NaChBac. ^{1}H magnetization transfer from NaChBac to isoflurane as a function of saturation times is further quantified as shown in Fig. 1*B*. The same STD experiment on a control sample, which had the same sample composition used for Fig. 1 but without NaChBac, showed no isoflurane STD signal (*SI Appendix*, Fig. S1). These results provide direct experimental support to the conclusions from previous functional measurements (10) and MD simulations (12) about direct isoflurane binding to NaChBac.

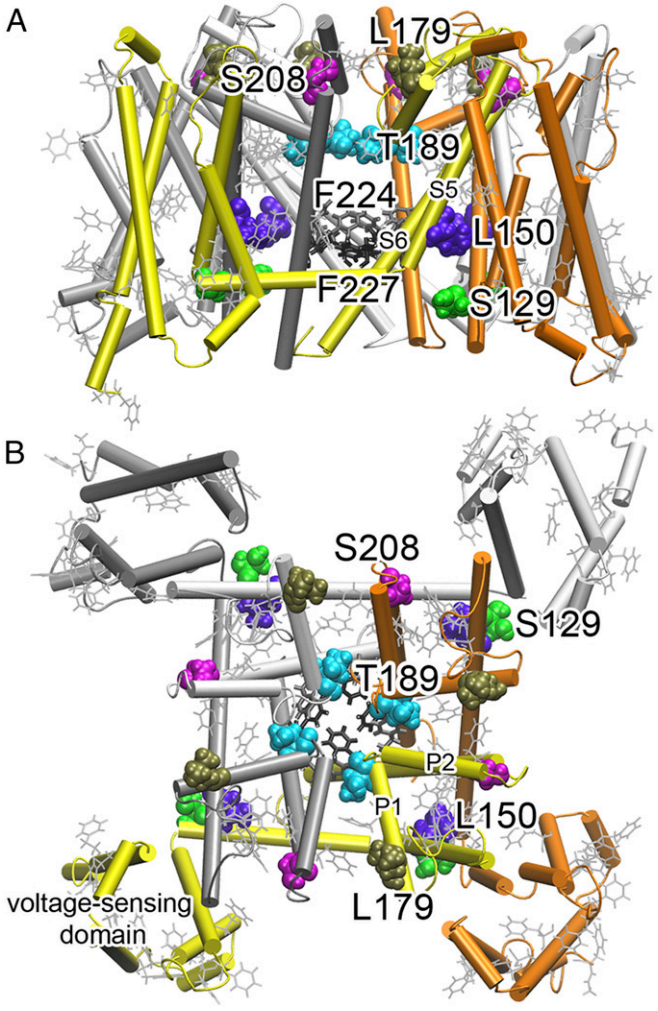

Fig. 2. Strategic labeling of NaChBac for ^{19}F NMR determination of isoflurane-binding sites. (*A*) A side view and (*B*) top view of ^{19}F-labeled residues. Colored residues shown in van der Waals presentation were mutated to cysteine individually and labeled with TET. Phenylalanine residues shown in gray lines were labeled with ^{19}F in their side chains (the meta position). There are a total of 25 phenylalanine residues in each monomer with 13 in the voltage-sensing domain. Note that the ^{19}F-labeled residues covered various regions of NaChBac: the extracellular surface (L179, S208), the selectivity filter (T189), the activation gate (F224, F227), the S4–S5 linker region (S129, L150), and the voltage-sensing domain.

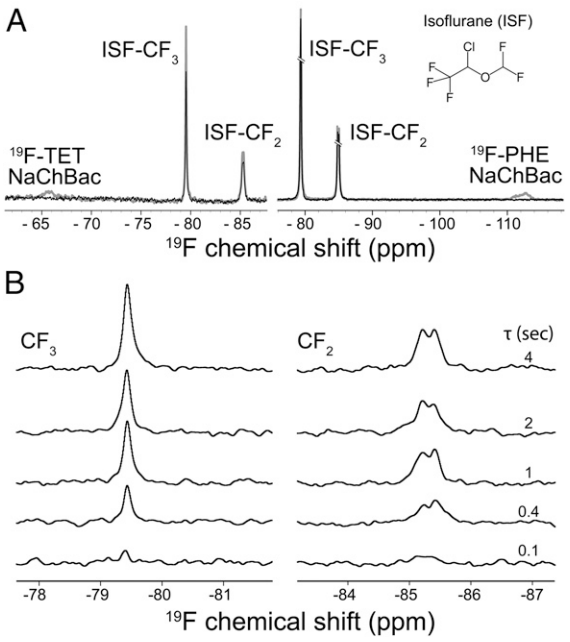

Fig. 3. ^{19}F NMR quantification of isoflurane binding to NaChBac. (*A*) A set of representative pairwise ^{19}F NMR spectra showing on-resonance (black, V_{on}) and off-resonance (gray, V_{off}) saturation of the ^{19}F TET-labeled T189C NaChBac (*Left*) and the ^{19}F PHE-labeled NaChBac (*Right*). The on- and off-resonance frequencies were –65.6 and –99.0 ppm for the ^{19}F TET (*Left*), –112.6 and –51.9 ppm for the ^{19}F PHE-labeled NaChBac (*Right*), respectively. ^{19}F chemical shifts were referenced to the trichlorofluoromethane resonance at 0 ppm. The saturation time was 4 s. (*Inset*) Isoflurane molecule. (*B*) Representative ^{19}F STD NMR spectra showing isoflurane interaction with the T189C NaChBac at various saturation times (τ). For each given saturation time, the STD spectrum (V_{STD}) results from subtracting the on-resonance spectrum from the off-resonance spectrum ($V_{STD} = V_{off} - V_{on}$). (*Left* and *Right*) Spectra from the $-CF_3$ and $-CF_2$ moieties of isoflurane, respectively.

Mapping Isoflurane Binding Sites in NaChBac. To identify specific isoflurane binding sites, we performed ^{19}F-NMR STD experiments on NaChBac labeled with ^{19}F probes to regions that were predicted by the MD simulations (12) (Fig. 2). As detailed in *Methods*, two ^{19}F-labeling strategies were used: (*i*) mutating specific residues, one at a time, to cysteine and covalently labeling them with a small fluorinated probe, 2,2,2-trifluoroethanethiol (TET) (16); or (*ii*) biosynthetically labeling all phenylalanine residues at once through expression incorporation of *m*-fluoro-DL-phenylalanine so that we can determine if isoflurane binds closely to any of the phenylalanine residues in NaChBac. We found that both strategies provided labeling efficiency of ∼20–40%, which was sufficient for ^{19}F-NMR STD experiments. Two-electrode voltage clamp electrophysiology measurements on *Xenopus* oocytes expressing NaChBac constructs indicated that channels with cysteine mutations for ^{19}F labeling retained similar functionality to that of the wild-type NaChBac, including voltage gating and isoflurane inhibition of channel activation (*SI Appendix*, Fig. S2).

^{19}F NMR signals of NaChBac (the TET labeling at –65.6 ppm and the phenylalanine labeling at –112.6 ppm) are distinct from those of isoflurane ($-CF_3$ at –79.5 ppm; $-CF_2$ at –85.4 ppm; Fig. 3*A*). In the ^{19}F STD experiments, ^{19}F signals of NaChBac labels were selectively saturated with on- and off-resonance saturation pulses alternatingly. ^{19}F STD signals of isoflurane, as shown in Fig. 3*B*, can be observed only if isoflurane has a close and steady contact with the ^{19}F probe in the protein to allow cross-relaxation of magnetization to occur. We quantified isoflurane interactions with individual regions of NaChBac (Fig. 4) using the method reported previously (13, 15, 17). The interaction strength, as quantified by the steady-state STD (STD_{max}) and the cross-relaxation rate constant (σ), are summarized in Table 1.

The S4–S5 linker site. S129 is located in the S4–S5 linker connecting the voltage-sensing domain (VSD) to the pore domain (PD) (Fig. 2). This residue pairs with L150 in the S5 helix of an adjacent subunit in forming a binding site for isoflurane. The ^{19}F STD results (Fig. 4*A* and Table 1) suggest a close and steady contact of isoflurane to both residues, particularly to S129, for which the average cross-relaxation rate σ is ∼5× that for L150. The distance between isoflurane to each of these two residues can be estimated based on $r_{S129}/r_{L150} = (\sigma_{L150}/\sigma_{S129})^{1/6}$, suggesting that isoflurane is ∼30% closer to S129 than to L150. MD simulations of isoflurane bound at this linker site show a preferential binding position that is more often in closer proximity to S129 than to L150 (Fig. 5).

Extracellular surface sites. Isoflurane was predicted to bind to sites near the extracellular surface of the channel at the interface between the P-loops (12). Both L179 and S208 are located in the extracellular interfacial region but have different microenvironments: S208 resides at the hinge of the P2 and S6 helices, whereas L179 is on the tip of the P1 helix with its side chain fully exposed to solvent (Fig. 2). The considerable difference in the STD_{max} values for these two residues (Fig. 4*B* and Table 1) suggest that isoflurane interacts more favorably with the S208 site than with the L179 site. The solvent exposure of the L179 side chain (Fig. 2) creates larger motional flexibility, which conceivably dampens the steady interaction of its side chain with isoflurane and results in a smaller STD.

Compared with the S4–S5 linker site, a notable difference at the extracellular surface sites is the apparent preferential binding orientation for isoflurane. At S208, both STD_{max} and σ are considerably greater for the $-CF_2$ moiety than for the $-CF_3$ moiety of isoflurane (Fig. 4*B* and Table 1). The data suggest a higher probability for the $-CF_2$ moiety to be saturated through cross-relaxation with the ^{19}F probe at the S208 position. Although the maximum saturating STD at L179 is small, the same orientational preference was detectable for L179 and was also observed for T189 in the ion selectivity filter, as described below.

Site at the base of the ion selectivity filter. T189 is located at the end of the P1 helix marking the cytoplasmic end of the ion selectivity filter (Fig. 2). Isoflurane shows not only a strong interaction with T189, but also a preferential orientation. The STD_{max} values for the $-CF_2$ and $-CF_3$ moieties of isoflurane are significantly different (Fig. 4*C* and Table 1), indicating a closer contact of the $-CF_2$ moiety to the T189 site and restricted motion of isoflurane in this region. $(STD_{max})_{CF2}/(STD_{max})_{CF3}$ and $\sigma_{CF2}/\sigma_{CF3}$ are significantly greater than 1 for the selectivity filter site and other extracellular sites. In contrast, these ratios are ∼1 at the S4–S5 linker region. Consistent with the NMR results, trajectories of the MD simulations showed a preferential orientation of isoflurane in the extracellular interface, but a much less pronounced orientation preference in the linker region (Fig. 6).

Phenylalanine in the pore and other regions of NaChBac. Inside the channel pore, F224 and F227 of the S6 helices in the tetramer form two phenylalanine rings (Fig. 2). F227 lines the pore near the cytoplasmic end and contributes to the channel activation gate (18, 19). In previous MD simulations, the F224 and F227 rings were found to hinder the diffusion of water molecules and Na^+ ions (20) and at least one isoflurane molecule occupied this pore region (12). Thus, we anticipated observation of significant STD effects in the NMR experiments at this site. To our surprise, only a subtle STD effect was detected (Fig. 4*C* and Table 1). The data seem to suggest that phenylalanine residues in NaChBac, including F227 and F224, do not produce a strong saturation transfer to isoflurane.

Discussion

It has long been proposed based on electrophysiology evidence that isoflurane binds to voltage-gated Na channels, including NaChBac, and that isoflurane-induced changes in channel function are relevant to isoflurane's anesthetic action (10, 21). Before

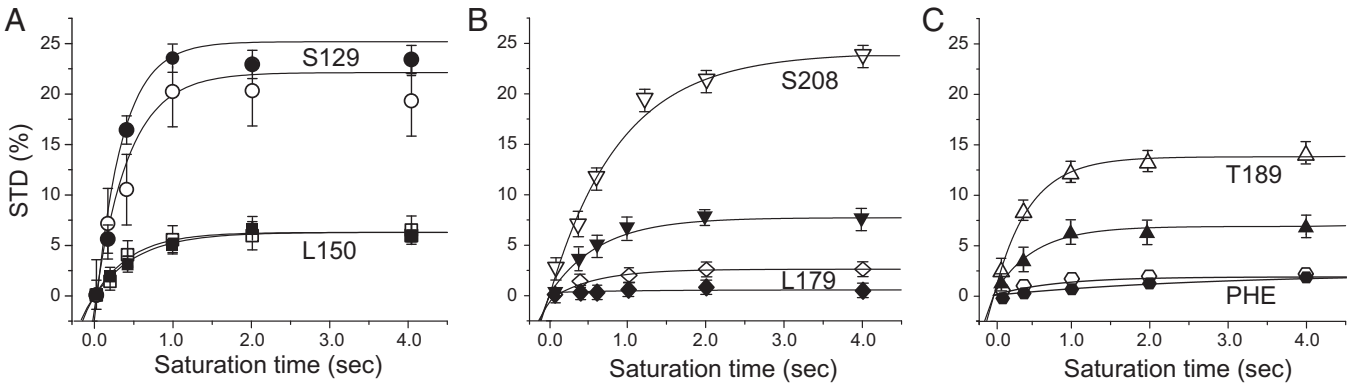

Fig. 4. Comparisons of ^{19}F NMR STD results as a function of saturation times in various regions of NaChBac. (*A*) The linker region (S129, ●; L150, ■), (*B*) the extracellular surface region (S208, ▼; L179, ♦), (*C*) the selectivity filter region (T189, ▲), and the PHE residues (⬢) in the pore region (F224, F227) and other regions of NaChBac. The filled and open symbols represent data from $-CF_3$ and $-CF_2$ moieties of isoflurane, respectively. The STD (%) uncertainties were calculated from the signal/noise ratios in the ^{19}F STD spectra. The solid lines represent the best fit of the experimental data by Eq. **1** (*Methods*). The fitting results are provided in Table 1.

the current study, few direct experimental data were available quantifying isoflurane binding to Na_V at atomic resolution. Through the site-directed fluorine atom placement as a source of energy transfer, the current study quantified the specific interactions between isoflurane and NaChBac using homonuclear ^{19}F STD values and intermolecular cross-relaxation rate constants. This method depends critically on the availability of a reliable structural model, either from experimental structures or from homology modeling. The success in the strategic placement of ^{19}F probes based on the predictions of potential isoflurane binding sites from MD simulations (11, 12) underscores the power of combining experimental NMR with computational simulations.

Our experimental results further differentiate the contributions from the multiple isoflurane binding sites to changes in channel function. Not all sites identified in the MD simulations have equal affinity for isoflurane. However, all potential isoflurane binding sites are amphipathic in nature (*SI Appendix*, Fig. S3). The S4–S5 linker site, bordered by S129 from one subunit and L150 from an adjacent subunit, shows strong isoflurane binding. Quantitative STD data show that isoflurane binds to both S129 and L150, with a 5:1 ratio in favor of S129. It has been suggested based on the crystal structure of Na_vAb (22) that the S4–S5 linker lies along the plane of the membrane interface to pivot the dilation of the central pore during gating. S129, corresponding to Q115 in Na_vAb, is located next to the pivot point between VSD and PD. Thus, interlocking two adjacent subunits in this region by an intervening isoflurane molecule is conceivably affecting the transmission of concerted motions from VSD to PD. Similarly, S208 is located at the hinge between the P2 helix and the pore-lining S6 helix. Isoflurane is found to interact strongly with S208 as a part of an intrasubunit binding site. The isoflurane binding to S208 likely affects the rigid-body motion of S6 and consequently the activation gate of Na_v channels as proposed previously (23–25).

The functional importance of the intersubunit pocket between S129 and L150 and the intrasubunit site near S208 is also evident in the electrophysiology measurements of the cysteine mutants used in this study. Cysteine mutations are in general well tolerated functionally, especially S→C and T→C mutations, unless the mutation-induced changes in side-chain packing or hydrophobicity profile occur at structural "hotspots" critical to function. Although the five mutants used in this study maintained the voltage-gating function and isoflurane sensitivity, they all showed a lower maximum channel current compared with the wild-type channel (*SI Appendix*, Fig. S2). Furthermore, unlike NaChBac channels expressed in the human embryonic kidney 293 cells (11), NaChBac and its mutants expressed in *Xenopus* oocytes do not demonstrate a strong sensitivity of the channel inactivation kinetics to isoflurane (*SI Appendix*, Fig. S4). There seems to be a dependence of inactivation kinetics on the location of the cysteine mutation. The S129C and L150C mutations located in the intersubunit isoflurane binding site decrease the characteristic time (τ) of channel inactivation, whereas the L179C, T189C, and S208C mutations located in the extracellular isoflurane binding site increase τ of channel inactivation (*SI Appendix*, Fig. S4).

The strong STD between isoflurane and T189 positively identified the existence of isoflurane within the channel pore. More importantly, the large difference in STD between $-CF_2$ and $-CF_3$ moieties suggests a restricted motion of the isoflurane molecule in the pore. Thus, isoflurane acts at least partially as a channel blocker to inhibit NaChBac channel function.

There are 25 phenylalanine residues in each NaChBac subunit (*SI Appendix*, Fig. S5). Based on the current structural model (Fig. 2), some of these phenylalanine residues are adjacent to

Table 1. STD fitting parameters

		Isoflurane-CF_3			Isoflurane-CF_2		
Regions	Residues	STD_{max}, %	k_{sat}, s^{-1}	$\sigma\times100$, s^{-1}	STD_{max}, %	k_{sat}, s^{-1}	$\sigma\times100$, s^{-1}
Linker	129	26.3 ± 0.6	2.7 ± 0.5	70 ± 13	20.5 ± 1.1	2.4 ± 1.1	49 ± 23
	150	6.3 ± 0.3	1.8 ± 0.4	11 ± 2.6	6.3 ± 0.4	2.1 ± 0.8	13 ± 5.1
Extracellular interface	179	0.52 ± 0.1	1.5 ± 0.9	0.8 ± 0.5	2.5 ± 0.1	1.8 ± 0.4	4.4 ± 1.0
	208	7.5 ± 0.4	1.6 ± 0.4	12 ± 3.1	24.0 ± 1.2	1.1 ± 0.3	26 ± 7.3
Filter pore	189	6.7 ± 0.3	2.0 ± 0.5	13 ± 3.4	14.0 ± 0.3	2.3 ± 0.3	32 ± 4.3
	PHE 224/227	1.3 ± 0.2	1.3 ± 1.0	1.6 ± 1.3	1.7 ± 0.3	1.4 ± 1.4	2.4 ± 2.4

Fitting results from Eq. **1** for the ^{19}F-NMR STD data in Fig. 4 covering several structural regions of NaChBac, including the linker region (S129 and L150), the extracellular interface (L179 and S208), the filter region (T189), and PHE residues in the pore (F224/F227) and other regions of NaChBac (Fig. 2). $\sigma = k_{sat} \times STD_{max}$.

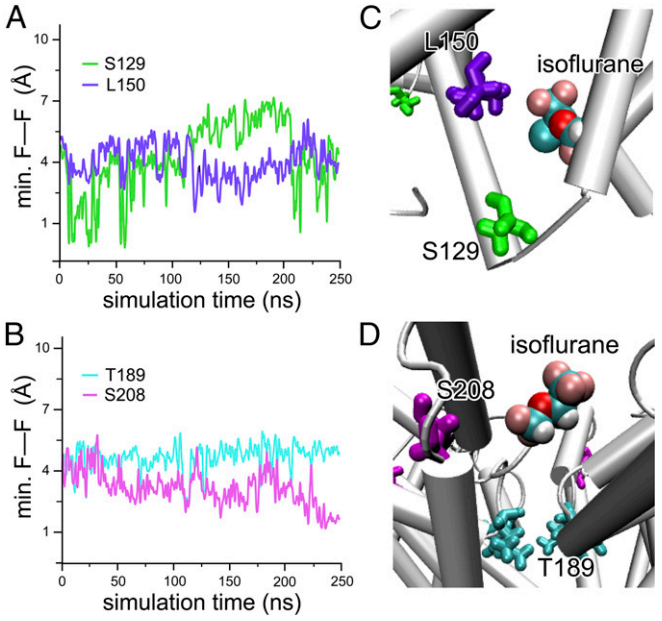

Fig. 5. MD simulations of isoflurane binding to NaChBac. Time evolution of the minimal distance between fluorine of the TET-labeled side chain and the fluorine atom of the nearest isoflurane molecule at (*A*) the linker sites, S129 (green) and L150 (purple), and (*B*) the selectivity filter site, T189 (cyan), and the extracellular surface site, S208 (magenta). Two independent MD simulations were performed and the corresponding time series were evaluated. In both cases, the isoflurane molecules stay close to the side chain of the S129- and S208-labeled positions, in agreement with the maximum STD observed in the NMR experiments. (*C* and *D*) Snapshots of the MD simulations showing the proximity of the isoflurane molecule to each of the labeled side chains. The isoflurane molecule is shown in van der Waals representation colored by atom type, and the protein side chain is shown as licorice using the same colors as in *A* and *B*.

S208 (i.e., F166 and F212) or in the opposite face of L179 from an adjacent subunit (i.e., F202) and hence would be expected to interact with isoflurane partially. However, because ^{19}F is only in the metaposition of the phenylalanine side chain, the STD effects are not detectable if the metaposition is not within 6 Å of the $-CF_2$ and $-CF_3$ moieties of isoflurane due to the steric hindrance of the aromatic ring structure. It appears that the single metasubstituted ^{19}F-phenylalanine labeling may have limited the STD detection. Therefore, caution should be exercised when interpreting the weak STD as a lack of isoflurane binding to phenylalanine residues.

Though the MD simulations narrowed our choices for site-directed placements of ^{19}F probes as sources of energy transfer in ^{19}F NMR experiments, we did not expect that simulations and NMR experiments would agree completely in all cases. Several methodology limitations should be noted. First, neither the choice of 1-palmitoyl-2-oleoyl-sn-glycero-3-phosphocholine (POPC) lipids in MD simulations nor the necessary use of detergents in high-resolution NMR experiments faithfully represents the native environment of NaChBac. However, because the primary goal of the current study is to use NaChBac as a structural homolog of eukaryotic Na_v channels to identify putative anesthetic binding regions, simulations in POPC allow a meaningful comparison of the results with previous studies on other voltage- and ligand-gated ion channels. Second, no experimental NaChBac structure is currently available, and the structural model used in this study was derived from comparative homology modeling based on the X-ray structure of Na_vAb, which was crystallized in a bicelle mixture of detergents and phosphatidylcholine lipids. Our simulations only captured a limited configuration space and the rotameric states of the side chains may not be fully sampled. Thus, the NaChBac structure itself can be a source of potential errors. Third, there is a timescale mismatch between simulation and NMR experiments. At some binding sites, anesthetic rotations and translations were fairly restricted, and we observed only few "flipping" events in the trajectories of duplicates of 250-ns simulations. A completely converged average over this degree of freedom cannot be assumed. At other sites, such as in the central pore cavity, anesthetics showed a rather fast rotational tumbling and translational diffusivity in the simulation (11). Such extreme mobility might reduce the cross-relaxation rate, rendering binding undetectable by STD. Despite these experimental limitations, the excellent qualitative agreement between simulation and NMR results allows us to conclude that isoflurane inhibits NaChBac by blocking the ion conduction at the base of the ion selectivity filter, restricting the pivot motions of the S5 and S6 helices, and interlocking two adjacent subunits in the S4–S5 inker region to affect the transmission of concerted motions from VSD to PD.

Methods

Protein and NMR Sample Preparation. NaChBac with a six-histidine tag and a TEV protease recognition site in the N terminus was expressed in *Escherichia coli* C41 cells (Lucigen) using the in-house expression vector pETHT at 18 °C for 24 h. Single cysteine mutations of selected residues, located near the N-terminal end of the S4–S5 linker (S129C), at the base of S5 helix interfacing the S4–S5 linker (L150C), at the extracellular interface near the hinge of the P1 helix (L179C), near the central pore at the bottom of the selectivity filter (T189C), and at the N-terminal hinge of the S6 helix (S208C), were performed individually using the QuikChange Lightning Mutagenesis kit (Agilent). Protein purification in n-dodecyl-β-D-maltoside (Anatrace) and subsequent labeling with TET to cysteine residues were conducted using similar protocols as reported previously (16). In addition to placing ^{19}F probes at the TET-labeled positions, we also introduced a ^{19}F probe to phenylalanine residues in NaChBac by biosynthetic incorporation of *m*-fluoro-DL-phenylalanine (Sigma) at a concentration of 50 mg/L in M9 media at 18 °C for 30 h.

NMR Data Acquisition and Analysis. ^{1}H STD spectra (13, 15) were collected in an interleaved fashion with the on- and off-resonance saturation frequencies of 0.4 ppm and 25 ppm, respectively. Saturation was achieved by a pulse train of 50-ms Gaus1.1000-shaped pulses with an interpulse delay of 4 μs. Saturation times were 0, 0.5, 1, 2, 4, 7, and 10 s. ^{19}F STD spectra were collected in a similar fashion. For the TET-labeled NaChBac, the spectral window was 30 ppm, the on- and off-resonance saturation frequencies were set at –65.6 ppm (TET-labeled residues) and –99.0 ppm, respectively. For

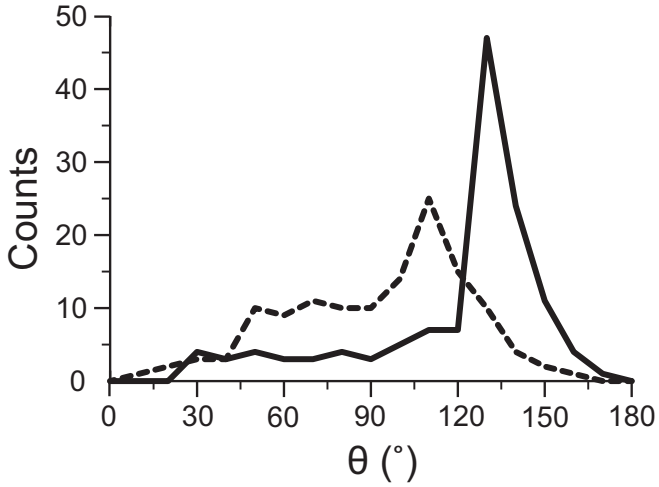

Fig. 6. Histograms of isoflurane orientations observed in MD simulations of isoflurane bound to NaChBac. A preferential orientation is observed for the isoflurane molecule in the extracellular binding sites surrounding the ion selectivity filter (solid line). The isoflurane molecule bound to the linker site shows a less-pronounced orientation preference (dashed line). The angle theta (θ) defines the orientation of the isoflurane CF_3–CF_2 molecular axis with respect to the membrane normal. The bin size of the histogram is 10°. 130 snapshots from a 250-ns simulation were used for the histogram.

^{19}F-phenylalanine–labeled samples, the spectral window was 59 ppm and the on- and off-resonance saturation frequencies were set at –112.6 ppm and –51.9 ppm, respectively. Saturation was achieved by a pulse train of 3-ms Q3.1000-shaped pulses with an interpulse delay of 3 ms. The total saturation times for the pulse train were 0.1, 0.4, 1, 2, and 4 s.

The STD data are fit to a monoexponential function (13, 17)

$$\mathrm{STD}(\%) = \mathrm{STD}_{\max}[1 - \exp(-k_{sat}t)], \quad [1]$$

where $\mathrm{STD}(\%) = (V_{off} - V_{on})/V_{off} \times 100\%$ V_{off} and V_{on} are the peak integrals from the off- and on-resonance saturation transfer NMR spectra; STD_{max} is the asymptotic maximum of the STD build-up curve; k_{sat} is the observed saturation rate constant; t is the saturation time. Note that $\mathrm{STD}_{max} = \sigma/k_{sat}$, where σ is the cross-relaxation rate constant between donor and receptor spins. Further details are provided in *SI Appendix*.

MD Simulations. We performed MD simulations of NaChBac using NAMD2.10 (26). The initial NaChBac model in a closed-pore conformation was obtained through comparative homology modeling based on the X-ray structure of Na_vAb (PDB ID code 3RVY) (22) and simulated in a fully hydrated lipid bilayer. The Na_vAb crystal structure features the voltage-sensor domains in the activated conformation and the pore domain in the closed conformation. Several lines of evidence (12, 20) suggest that such a structure might be representative of an inactivated state. Therefore, we consider our structure a reasonable model of NaChBac in the inactivated state. To better model the conditions in the ^{19}F-NMR experiments, separate in silico mutations of S129 and L150 to cysteines and attachment of the TET ^{19}F probe were performed using the last frame of the previous isoflurane-flooding MD simulation of the wild-type NaChBac (12), from which most isoflurane molecules were removed except those in the experimentally suggested binding sites. For both mutant systems, four putative binding pockets in the tetramer were occupied by three isoflurane molecules each (12 in total) in the starting configuration, using the final frame from a previous work (12). The two systems were simulated for 250 ns in four independent runs (two for each system) to ascertain robustness and reproducibility of the results. For the isoflurane binding sites at the extracellular interface, the previously published simulation trajectories (12) were analyzed. Further details are provided in *SI Appendix*.

Functional Studies with NaChBac Mutants. NaChBac RNA was prepared from the pPoL vector (a gift from Manuel Covarrubias's laboratory at Thomas Jefferson University) using the mMessage mMachine T7 kit (Ambion) and purified with the RNeasy Kit (Qiagen). Single cysteine mutations were introduced using the same method as that for the NMR samples. NaChBac constructs were expressed in *Xenopus* oocytes by injecting 25–50 ng of the RNA into stages 5–6 oocytes. Further details are provided in *SI Appendix*.

ACKNOWLEDGMENTS. This work was supported by National Institutes of Health Grants R37GM049202, R01GM056257, T32GM075770, and P01GM055876.

1. Zhou DW, Mowrey DD, Tang P, Xu Y (2015) Percolation model of sensory transmission and loss of consciousness under general anesthesia. *Phys Rev Lett* 115(10):108103.
2. Tang P, Xu Y (2002) Large-scale molecular dynamics simulations of general anesthetic effects on the ion channel in the fully hydrated membrane: The implication of molecular mechanisms of general anesthesia. *Proc Natl Acad Sci USA* 99(25):16035–16040.
3. Eckenhoff RG, Johansson JS (1997) Molecular interactions between inhaled anesthetics and proteins. *Pharmacol Rev* 49(4):343–367.
4. Campagna JA, Miller KW, Forman SA (2003) Mechanisms of actions of inhaled anesthetics. *N Engl J Med* 348(21):2110–2124.
5. Franks NP, Lieb WR (1994) Molecular and cellular mechanisms of general anaesthesia. *Nature* 367(6464):607–614.
6. Herold KF, Hemmings HC, Jr (2012) Sodium channels as targets for volatile anesthetics. *Front Pharmacol* 3:50.
7. Hemmings HC, Jr, et al. (2005) Emerging molecular mechanisms of general anesthetic action. *Trends Pharmacol Sci* 26(10):503–510.
8. Purtell K, Gingrich KJ, Ouyang W, Herold KF, Hemmings HC, Jr (2015) Activity-dependent depression of neuronal sodium channels by the general anaesthetic isoflurane. *Br J Anaesth* 115(1):112–121.
9. Covarrubias M, Barber AF, Carnevale V, Treptow W, Eckenhoff RG (2015) Mechanistic insights into the modulation of voltage-gated ion channels by inhalational anesthetics. *Biophys J* 109(10):2003–2011.
10. Ouyang W, Jih TY, Zhang TT, Correa AM, Hemmings HC, Jr (2007) Isoflurane inhibits NaChBac, a prokaryotic voltage-gated sodium channel. *J Pharmacol Exp Ther* 322(3):1076–1083.
11. Barber AF, Carnevale V, Klein ML, Eckenhoff RG, Covarrubias M (2014) Modulation of a voltage-gated Na+ channel by sevoflurane involves multiple sites and distinct mechanisms. *Proc Natl Acad Sci USA* 111(18):6726–6731.
12. Raju SG, Barber AF, LeBard DN, Klein ML, Carnevale V (2013) Exploring volatile general anesthetic binding to a closed membrane-bound bacterial voltage-gated sodium channel via computation. *PLOS Comput Biol* 9(6):e1003090.
13. Mayer M, Meyer B (1999) Characterization of ligand binding by saturation transfer difference NMR spectroscopy. *Angew Chem Int Ed* 38(12):1784–1788.
14. Wagstaff JL, Taylor SL, Howard MJ (2013) Recent developments and applications of saturation transfer difference nuclear magnetic resonance (STD NMR) spectroscopy. *Mol Biosyst* 9(4):571–577.
15. Bondarenko V, Yushmanov VE, Xu Y, Tang P (2008) NMR study of general anesthetic interaction with nAChR beta2 subunit. *Biophys J* 94(5):1681–1688.
16. Kinde MN, et al. (2015) Conformational changes underlying desensitization of the pentameric ligand-gated ion channel ELIC. *Structure* 23(6):995–1004.
17. Mayer M, James TL (2004) NMR-based characterization of phenothiazines as a RNA binding scaffold. *J Am Chem Soc* 126(13):4453–4460.
18. Kuo CC, Liao SY (2000) Facilitation of recovery from inactivation by external Na+ and location of the activation gate in neuronal Na+ channels. *J Neurosci* 20(15):5639–5646.
19. Townsend C, Horn R (1999) Interaction between the pore and a fast gate of the cardiac sodium channel. *J Gen Physiol* 113(2):321–332.
20. Barber AF, et al. (2012) Hinge-bending motions in the pore domain of a bacterial voltage-gated sodium channel. *Biochim Biophys Acta* 1818(9):2120–2125.
21. OuYang W, Hemmings HC, Jr (2007) Isoform-selective effects of isoflurane on voltage-gated Na+ channels. *Anesthesiology* 107(1):91–98.
22. Payandeh J, Scheuer T, Zheng N, Catterall WA (2011) The crystal structure of a voltage-gated sodium channel. *Nature* 475(7356):353–358.
23. Amaral C, Carnevale V, Klein ML, Treptow W (2012) Exploring conformational states of the bacterial voltage-gated sodium channel NavAb via molecular dynamics simulations. *Proc Natl Acad Sci USA* 109(52):21336–21341.
24. Vargas E, et al. (2012) An emerging consensus on voltage-dependent gating from computational modeling and molecular dynamics simulations. *J Gen Physiol* 140(6):587–594.
25. Zhang X, et al. (2012) Crystal structure of an orthologue of the NaChBac voltage-gated sodium channel. *Nature* 486(7401):130–134.
26. Phillips JC, et al. (2005) Scalable molecular dynamics with NAMD. *J Comput Chem* 26(16):1781–1802.